Universitat Politècnica de Catalunya (UPC)
Universitat Autònoma de Barcelona (UAB)
Universitat de Barcelona (UB)
Institut de Ciències Fotòniques (ICFO)

http://www.photonicsbcn.eu

Master in Photonics

MASTER THESIS WORK

QUANTUM CONTROL OF COLD ATOMS USING MICROWAVES

Ferran Martin Ciurana

Supervised by Dr. Morgan W. Mitchell, (ICFO)

Presented on date 8th September 2011

Registered at

Escola Tècnica Superior d'Enginyeria de Telecomunicació de Barcelona

Quantum control of cold atoms using microwaves

Ferran Martin Ciurana

ICFO-Institut de Ciencies Fotoniques, Mediterranean Technology Park, Av. Carl Friedrich Gauss, 3, 08860 Castelldefels (Barcelona), Spain

E-mail: ferran.martin@icfo.es

Abstract. We study quantum control of the ground hyperfine manifold of alkali-metal atoms based on applied microwave fields. We performed microwave spectroscopy both in the frequency and the time domain resulting in the observation of spectra and Rabi oscillations. We also apply a spin echo technique to characterize the coherence time of our trapped atoms.

Keywords: Quantum control, microwave spectroscopy, spin echo, broadening

1. Framework

Coherent control over quantum systems is increasingly important in a variety of fields including computation [1], metrology [3], chemical dynamics [4] and others [5]. Such control open the doors to a variety of applications and allows us to perform some tasks that would otherwise be intractable. For instance, computers which can make use of quantum coherence could be able to solve certain problems much faster than any classical computer. Metrology is another area in which coherent control offers advantages. It has been shown that full quantum control allows greater sensitivity in parameter estimation than the "standard quantum limit" as the number of particles is increased [2]. Control over chemical dynamics has greatly improved as a result of applying ideas from coherent control.

In this thesis, we will focus on control of trapped neutral atoms. We explore the idea of coherent control to manipulate the population of the ground hyperfine manifold of trapped ultra-cold atoms. In our case, we work with an atomic sample that has a length of 10mm. The major source of decoherence is inhomogeneous magnetic fields, and due to our sample length becomes a challenge for coherently control.

We first describe the atomic physics relevant to microwave spectroscopy of rubidium-87, then the experimental apparatus used to apply microwave pulses to the atoms. A sequence of spectroscopic studies of a cold rubidium cloud in an optical dipole trap is done.

2. Atomic physics

2.1. Level structure in magnetic fields

^{87}Rb is a "first row" alkali metal having only a single electron in its valence shell. The hyperfine structure **F** results from the coupling between the total angular momentum **J**=**L**+**S** together with the total nuclear angular momentum **I** given by $\mathbf{F} = \mathbf{J} + \mathbf{I}$ and can take the values $|J-I| \leq F \leq J+I$. In the ^{87}Rb ground state $J = 1/2$ and $I = 3/2$. Hence, $F = 1$ or $F = 2$. If an external magnetic field is applied the degeneracy of the $2F + 1$ magnetic sub-levels is lifted, known as Zeeman splitting. The Hamiltonian of this interaction is [7]

$$H_B = \frac{\mu_B}{\hbar}(g_S\mathbf{S} + g_L\mathbf{L} + g_I\mathbf{I}) \cdot \mathbf{B} \tag{1}$$

where μ_B is the Bohr magneton, $g_S \simeq 2$, $g_L \simeq 1$, $g_I = -0.000995$ are the electron spin, electron orbital, and nuclear Landé g-factors, respectively.

In the case that energy shift due to the magnetic field is small compared to the hyperfine splitting, F is a good quantum number and the interaction Hamiltonian can be written as:

$$H_B = \mu_B g_F F_z B_z \tag{2}$$

since it is applied in the z-axis. This first order linear equation in B also neglects the nuclear term g_I since is much smaller than g_J, and

$$g_F \simeq g_J \frac{F(F+1) - I(I+1) + J(J+1)}{2F(F+1)} \tag{3}$$

The corresponding energy shifts between the magnetic sub-levels is

$$\Delta E_{|F,m_F\rangle} = \mu_B g_F m_F B_z \tag{4}$$

2.2. Magnetic transitions

The hyperfine interaction in ^{87}Rb splits the $5S_{1/2}$ ground state in two sub-levels $F = 1$ and $F = 2$. In the case of zero external magnetic field, the frequency difference between these levels is $\omega_{|F=1\rangle \leftrightarrow |F'=2\rangle} = 2\pi \cdot 6,834,682,610$ Hz and it is used as an atomic reference frequency standard. Direct transitions between these two states are driven by magnetic dipole interactions in the microwave regime, as the electric dipole transition is forbidden between two **S** states. The magnetic dipole potential is

$$V = -\mu \cdot \mathbf{B} \tag{5}$$

For an alternating magnetic field linearly polarized like the radiation we expect from our antenna (see section 3.3) we have

$$\mathbf{B} = B_1 \cos(\mathbf{k} \cdot \mathbf{r} - \omega t)\hat{\mathbf{x}} \tag{6}$$

where **r** represents the atom center of mass point which we will take as zero for convenience and $\hat{\mathbf{x}}$ is a unit vector in the x direction. As the ground state hyperfine

levels are both S-states ($L = 0$), only the terms μ_S and μ_I contribute to the interaction energy:

$$V = \frac{B_1}{\hbar}(\mu_B g_S S_z + \mu_N g_I I_z)\cos(\omega t) \tag{7}$$

The calculation of this potential for the clock transition gives

$$\frac{-B_1}{2}(\mu_B g_S + \mu_B g_I)\cos(\omega t) \tag{8}$$

and therefore the single photon Rabi frequency is

$$\Omega = \frac{-B_1}{2\hbar}(\mu_B g_S + \mu_B g_I) \tag{9}$$

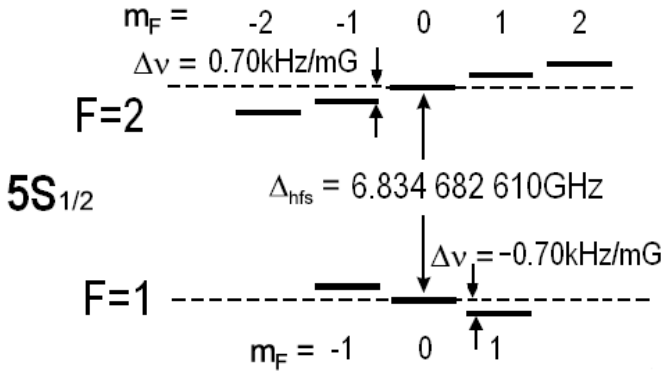

Figure 1. Diagram of the ground hyperfine level structure of ^{87}Rb

3. Experimental methods

Sophisticated methods and highly technical experimental requirements are needed to get atoms trapped. Since they are the prerequisite for correct study of microwave spectra but not the objective of the work here presented, I will present briefly the system for trapping and preparing cold atomic ensembles, and focus on the microwave parts. Detailed explanations of cooling and trapping atoms can be found in several textbooks and review publications, for example [6].

3.1. Setup

The basic experimental setup is shown in Figure 2. We use a double stage magneto-optical trap (MOT). Atoms are accumulated in a two-dimensional MOT which continuously feeds a three dimensional MOT. A single-beam optical dipole trap is overlapped with the 3D MOT. After loading, the gradient fields and trapping beams of the 2D and 3D MOT are turned off, leaving the atoms in an all-optical trap, where the microwave study takes place. All measurements rely on counting the number of atoms in the excited state F=2 after we apply the microwave signal, knowing the total number of atoms we load in the trap and their initial state distribution. We count the number of

atoms through absorption image. Atomic absorption casts a shadow which is detected by the CCD camera. A microwave antenna is placed close to the vacuum cell. Since the experiments are very sensitive to magnetic fields, we use three orthogonal pairs of coils to compensate the earth's magnetic field. The compensation coils of the z-axis also serve to produce a guiding field, which defines the quantization axis.

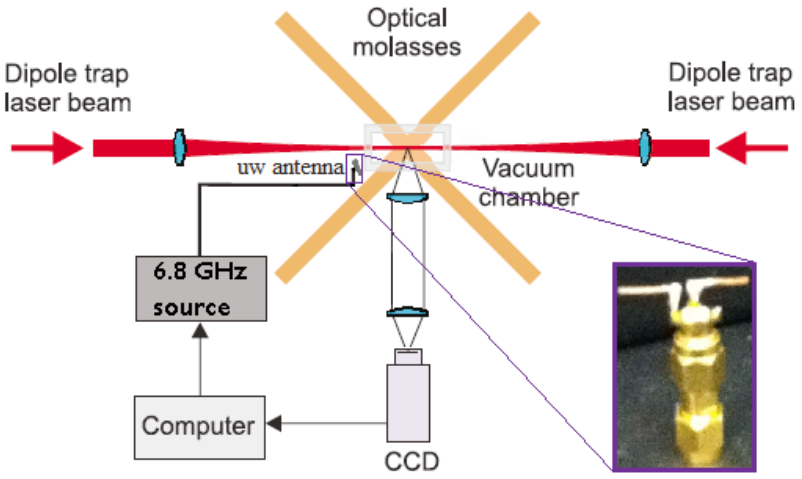

Figure 2. Scheme of the experimental setup. A powerful and gently focused laser, the dipole trap, is superimposed with the atomic cloud of the 3D MOT. We shine resonant microwave radiation on the trapped atoms. Using the information of the absorbtion image a computer calculates the corresponding number of atoms excited. Close-up view of the dipole antenna

3.2. 6.8 GHz source

Since the Direct Digital Synthesizer (DDS) on the market able to reach frequencies of several GHz are very expensive and are designed for other proposes, the microwave signal is generated in two steps. We use an atomic clock to generate a precise signal at a fixed frequency and mix this with a DDS for flexibility.

The atomic clock, Stanford Research SRS 635, is set to $f_{clock} = \frac{1}{4}\Delta_{hfs} - 300$ MHz. All the harmonics are filtered except the fourth. The frequency separation between the harmonics is sufficiently large for using standard Minicircuits filters. The carrier frequency is then mixed with the signal produced by a DDS to generate the microwave signal at the hyperfine splitting frequency of ^{87}Rb. The DDS used is an AD9910 from Analog Devices. The frequency mixer used is a ZX05-73L+ from Minicircuits. This frequency mixer have relatively low conversion losses and good isolation between the Local Oscillator and the output. Even so, a cavity band pass filter is placed at the output of the mixer. The signal is then amplified by a series of two amplifiers. A pre-amplification, using the model ZX80-8008E+, followed by a power amplifier, ZVW-3W-183+, which finally brings the signal to 35 dBm.

3.3. Microwave antenna

At the beginning of this project different types of antennae were considered and investigated, and finally we settled on working with a half-wave dipole antenna. We prioritized having the largest intensity on the atoms by having the smallest distance between atoms and antenna even though the major part of the signal won't be felt by the atoms. The small size of the half-wave dipole antenna (2.2 cm long and 1 cm tall) allows us to place it at a distance of few millimeters from the atoms.

The antenna was made by welding two pieces of copper of 0.5 mm thickness in a male-male SMA connector. One technical requirement to transfer the signal efficiently is the aspect of impedance mismatch; the antenna must have 50 Ω input impedance. The length of the antenna is reduced to 0.48λ in order to have a real input impedance. We characterized the reflected signal using a spectrum analyzer (Rohde & Schwarz FPS 13) and a circulator (Ditom microwave inc.). We saw that the difference between the input power and the reflected signal is above 20 dB, showing that the antenna is resonant at the frequency of 6.8 GHz. The antenna impedance is calculated with the values of the reflected and input signals, being $99.70 \pm 0.05\,\Omega$, a bit larger than the typical value for a half-wave dipole antenna impedance, $\sim 73\,\Omega$. Its FWHM is of 5 MHz.

The most effective position for the antenna was found empirically by maximizing the Larmor precession manually adjusting the antenna distance from the vacuum cell.

4. Microwave spectroscopy

As well as the possibility of coherent manipulation of the ground state hyperfine levels, microwaves are also valuable as a sensitive probe for level shifts due to magnetic fields. This allows us to precisely calibrate externally applied fields.

We performed microwave spectroscopy both in the frequency and the time domain resulting in the observation of spectra and Rabi oscillations, respectively.

4.1. Spectroscopy of the hyperfine transitions

By optical pumping atoms are prepared to be in a thermal distribution (all sub-levels equally occupied) in the ground F=1 state. The frequency splitting between hyperfine levels is ± 0.70 kHz/mG for F=2 (F=1), see Figure 1. The current applied to the z-coils was 100 mA. By scanning the frequency in the vicinity of the transition frequencies we expect to observe the resonances. The total span of the frequency scan is 200 kHz with a step size of 5 kHz. Each point is averaged over 3 shots with a total number of atoms trapped in F=1 of about 400,000 each time. Figure 3 shows the spectrum for square pulse of 300 μs duration at maximum power.

We can be observe 7 peaks since some frequencies correspond to more than one transition. Different initials and finals hyperfine states globally are affected by the same frequency splitting, making them degenerate transitions. We drive at the same time $|F' = 1, m_F = 1\rangle \rightarrow |F' = 2, m'_F = 0\rangle$ and $|F = 1, m_F = 0\rangle \rightarrow |F' = 2, m'_F = -1\rangle$,

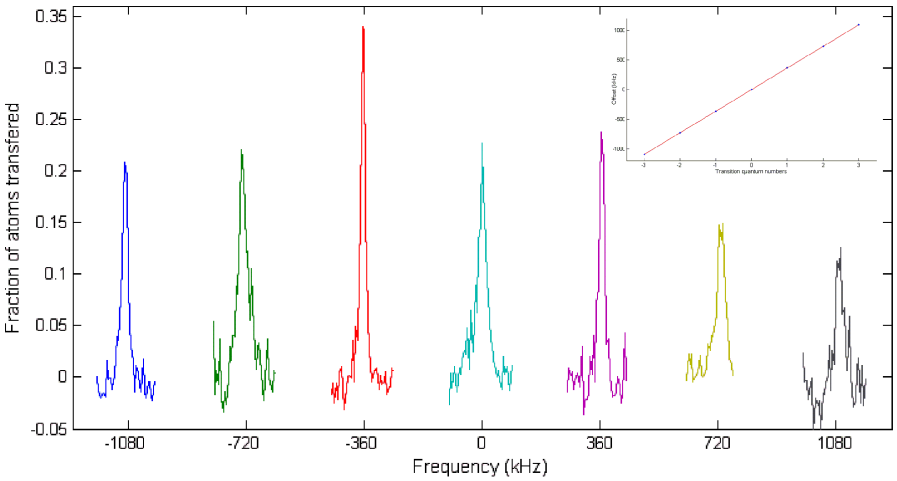

Figure 3. Spectrum of the hyperfine ground state of ^{87}Rb for a thermal state and $t_{\mu w}$=0.3ms, taking the clock frequency as the origin.

	-1 to -2	-1 to -1	0 to -1	0 to 0	0 to 1	1 to 1	1 to 2
Offset (kHz)	-1090± 0.3	-729.2± 0.9	-362.8± 0.2	0.55± 0.67	365.7± 0.2	729.8± 0.6	1091± 1.1
FWHM (kHz)	21.6± 0.7	39.9± 1.9	15.7± 0.4	34.4± 1.4	19.6± 0.8	30.1± 0.9	25.7± 1.7
Peak	0.21±0.01	0.22±0.01	0.34±0.01	0.23±0.01	0.24±0.01	0.15±0.01	0.13±0.01

Table 1. Data from the fittings for the hyperfine transitions.

and also $|F = 1, m_F = 1\rangle \rightarrow |F' = 2, m'_F = 0\rangle$ together with $|F = 1, m_F = -1\rangle \rightarrow |F' = 2, m'_F = 0\rangle$. For this reason these peak involves more transference of atoms than the others. The antenna was placed perpendicular to the atomic cloud, so due to the antenna polarization the π transitions should be more efficient than the σ ones. However, we can see both types of transitions with comparable atoms transfer rates.

From equation 4 a linear behavior is expected in the separation of the levels. This result is confirmed and plotted in Figure 3, inlaid. The positions of the peaks are obtained by fitting the spectrum of each transition. The values of the widths indicates that there is a source of broadening. This can be clearly seen in the clock transition. The precision of atomic clocks relies on the fact that this hyperfine transition is extremely narrow, rather limited by technical reasons than by the natural linewidth. Some result of these fittings are presented in Table 1.

Different sources of broadening can act simultaneously such as power broadening, broadening due to finite time the μw signal is applied, inhomogeneous coupling between the cloud and the antenna, inhomogeneous energy distribution of the atoms, collisions between atoms, among others. We expect that some of them can be negligible, like atom collisions since our atomic cloud is quite dilute, while other have a strong presence.

The origin of power broadening relies in the strong coupling between the line shape of the transition and the driven field, enlarging the transition line shape. To avoid power broadening, we used an attenuator that reduced the intensity coming from the DDS by

	clock	1 to 1	1 to 2
FWHM (kHz)	8.18± 0.04	10.03± 0.11	10.82± 0.05
Peak	0.97±0.01	0.67±0.01	0.47±0.01

Table 2. Results from the narrower scan of the selected transitions. The origin of frequencies is different for each transition, taking the origin according to the previous offset results. Also the clock transition is re-normalized to the number of atoms we can address

Origin	expression	clock	1 to 1	1 to 2
Power (kHz)	$\sqrt{2}\Omega$	6.02±0.03	4.85 ± 0.02	5.75 ± 0.03
Pulse bandwidth (kHz)	$\frac{1}{2\pi\Delta t}$	1.06± 0.04	1.06± 0.04	1.06± 0.04

Table 3. Homogenous broadening mechanism and estimated effect.

20 dB. In this context, the scanning of the transitions was repeated, but only for the clock transition, the 1 to 1 and for the 1 to 2. The microwave was applied 0.1 ms, each point was averaged 10 times and each step was of 200 Hz. For the clock transition, the state was initially prepared into a thermal state, while for the other two the initial state was a polarized state, all atoms in $m_F = 1$.

In Figure I [left] we can see the spectra of these transitions. Although broadening has been reduced, the peaks still have a large width. Power broadening is still be present, but other mechanisms like field or light-shift inhomogeneities are now visible.

Even though that the μw was applied for a short period of time (smaller than a π-pulse length) we can transfer a large quantity of atoms to the excited state, specially for the clock transition where we can transfer almost all the atoms those we have access, close to 1. This data are re-normalized since in a thermal state we can only address to 1/3 of the atoms.

4.2. Rabi flopping

Rabi oscillations are coherent temporal oscillations of the population. The study of the Rabi oscillations can give us information about the presence of inhomogeneities. In order to observe Rabi oscillations, we set the synthesizer to the atomic resonance frequency we want to study. We study Rabi oscillations of the clock transition, the 1 to 1, and the 1 to 2. Following the same procedure as before, we optically pump the atoms into the F = 1 with no net polarization for the clock transitions, while for the others atoms have positive polarization. Varying the pulse length from 5 μs to 1 ms in steps of 25 μs, leading to the observation of Rabi oscillations, see Figure I [right]. Each point in the graph results from averaging 10 times.

Having the details on the Rabi flopping we can estimate better the action of power broadening. Following [7] we calculate that the power broadening = $\sqrt{2}\Omega$, where Ω is the Rabi frequency. At the same time we also expect broadening due to the finite time the μw is applied, being these effects homogeneous, Table 3.

	clock	1 to 1	1 to 2
Frequency (kHz)	4.25±0.02	3.43± 0.02	2.87 ± 0.02
$\mathbf{t}_{decay}$ (ms)	0.230 ± 0.107	0.374 ± 0.153	0.603 ± 0.375
B (mG)	4.83×10^{-4}	$3.90\ \times10^{-4}$	3.26×10^{-4}

Table 4. Data from Rabi oscillations.

We expect some inhomogeneous broadening due to ac Stark-shift of atoms in the dipole trap. However, it is difficult to get a calculation for such effect. At some point its presence should also appear.

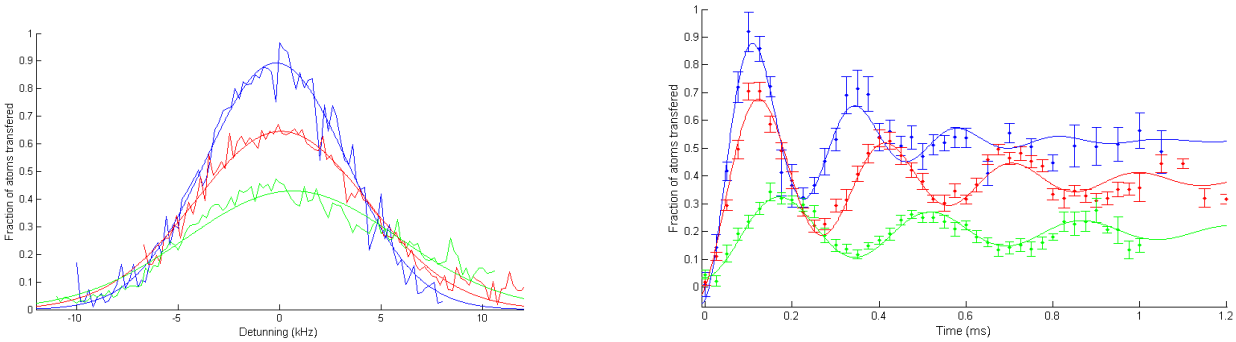

Figure I. Experimental points and fittings for the studied cases: clock (blue), 1 to 1 (red) and 1 to 2 (green). Left: Narrower scan for the selected transitions. Right: Experimental observation of Rabi flopping. Data re-normalized for the clock transition.

Inhomogeneous effects are responsible of the attenuation of the Rabi oscillations. This damping is due to driving field inhomogeneities, resulting in a coherence time of $\approx 200\mu$s for the clock transition, the transition insensitive to magnetic fields. A damped oscillation was fitted to the data, giving best-fit parameters shown in Table 6. From this fitting we can retrieve the characteristics of the flopping, Table 4

5. Spin echo

One useful experiment is spin echo. It is a pulse sequence of resonant radiation that permits us to study the time scale of spin-spin interactions and other effects leading on loss of phase coherence [8]. In our case we have to apply an extra $\pi/2$ pulse to measure the system response. Figure 4 shows and explains the details.

If the inversion pulse is applied after a period t of dephasing, the inhomogeneous evolution will rephase to form an echo at time $2t$. The intensity of the echo relative to the initial signal is given by $e^{(-2t/T_2^*)}$, where T_2^* is the time constant for spin-spin relaxation and other imperfections.

The inhomogeneous dephasing predominantly arises due to local magnetic field inhomogeneities along the distribution of the atoms in the trap. From this result we can retrieve the irreversible dephasing causing the decay of the spin echo. Studying spin

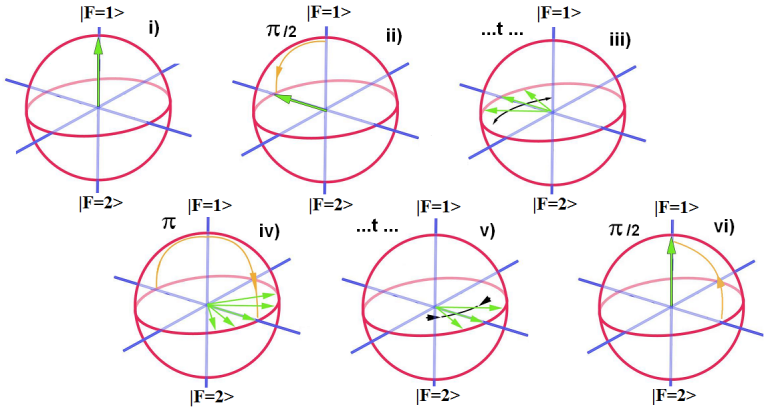

Figure 4. The experimental spin echo sequence: i)Initially all spins are vertical oriented. ii) A $\pi/2$ pulse that flips the spins in the equatorial plane is applied. iii) Spins evolve freely following local B-inhomogeneities. iv) A π pulse is applied so to reverse spins spreading. v) spins are refocused. vi) Complete refocusing and a $\pi/2$ pulse to measure the strength of the magnetization.

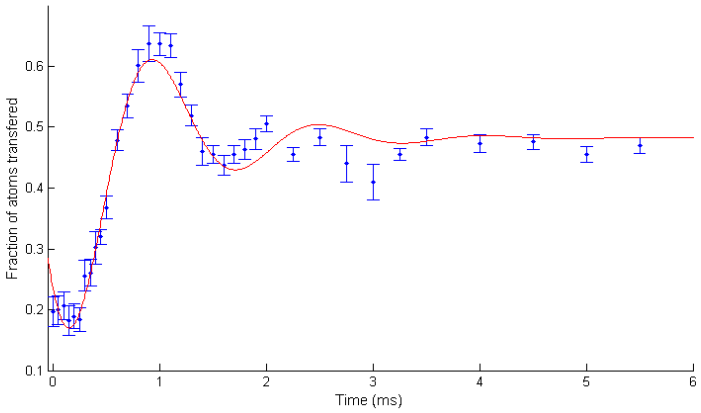

Figure 5. Experimental observation of spin echo with imperfect pulses.

Origin	expression	Value
Damping	$T_{coherence}$	$\approx 350\mu s$
Relaxation	T_2^*	$\approx 0.90ms$

Table 5. Inhomogenous broadening mechanism and estimated coherence times.

echo between the 1 to 1 transition, see Figure 5, we got that $T_2^* = 0.88 \pm 0.23$ ms, the frequency was 640 ± 14 Hz and the peak 0.64 ± 0.01. The spin echo signal oscillates at the frequency difference between the resonant frequency and the driven one. The echo doesn't reach the maximum because the applied pulses were too short, $\pi/2$= 60 (73), π= 120 (146), in ms. In parenthesis the values calculated from Rabi results.

The origin of the echo signal and its oscillation remains unclear at this point and would require a more investigation.

Equation: $a \cdot e^{-bt} \sin(dt + c) + e$					
	a	b	c	d	e
clock	0.19±0.06	4.47 ±2.05	26.73 ± 2.4	-1.50 ± 0.39	0.18 ± 0.01
1 to 1	0.41±0.11	2.68±1.10	21.57 ±1.12	-1.2±0.29	0.39 ± 0.02
1 to 2	0.17± 0.06	1.66 ±1.03	18.05±1.11	-1.60 ±0.40	0.20 ±0.02
Spin echo	0.39 ± 0.10	1.14 ± 0.51	4.02 ± 0.53	-2.45 ± 0.32	0.48 ± 0.024

Table 6. Values for damped oscillation fitting. Error represents 95% confidence.

6. Conclusions

In this work we have demonstrated the possibility of coherently manipulating the ground state hyperfine levels using microwave radiation, treating the atomic ensemble as a whole. Using spectroscopic techniques, we have successfully recorded microwave spectra. We observed Rabi oscillations with excellent fringe visibility and Rabi frequencies of about ≈ 5 kHz even with an attenuated signal. This allows us to apply π and $\pi/2$ pulses, which confirm our atomic state control. Finally we used this pulses to perform spin echo experiment. All this three spectroscopic methods permitted us to identify different kinds of broadening, both homogeneous and inhomogeneous.

Acknowledgments

I am deeply indebted to my tutor Prof. Morgan Mitchell for giving me the opportunity to participate in a so exciting project. I want to thank my supervisor Rob Sewell for all his help throughout this work. Special mention to Mario Napolitano for his invaluable support and guidance in and out the lab.

7. Bibliography

[1] M. A. Nielsen and I. L. Chuang, *Quantum Computation and Quantum Information*, 1st edition, Cambridge University Press, 2000.

[2] V. Giovannetti, S. Lloyd, and L. Maccone, *Quantum-Enhanced Measurements: Beating the Standard Quantum Limit*, Science 306, 1330 (2004).

[3] M. Napolitano, et al. *Interaction-based quantum metrology showing scaling beyond the Heisenberg limit*, Nature 471, 486-489, (2011)

[4] H. Rabitz, *CHEMISTRY: shaped laser pulses as reagents*, Science 299 (2003), 525-527.

[5] Mischuck, B and Deutsch, I.H. *Coherent control of atomic transport in spinor optical lattice*, Phys. Rev. A 81, 023403 (2010)

[6] M. Schulz. *Tightly confined atoms in optical dipole traps.* Ph.D. thesis (2002).

[7] D.A. Steck, *http://atomoptics.uoregon.edu/d̃steck/teaching/quantum-optics/quantum-optics-notes.pdf*

[8] Hahn, E.L., *Spin echoes*, Phys. Rev. 80, 580-594 (1950)